JOC The Journal of Organic Chemistry

Article

pubs.acs.org/joc

# Reaction Pathways for the Thermal Decomposition of Methyl Butanoate

Mohamad Akbar Ali and Angela Violi*

Department of Mechanical Engineering, University of Michigan, Ann Arbor, Michigan 48109-2125, United States

Supporting Information

**ABSTRACT:** In recent years, biodiesel fuels, consisting of long-chain alkyl (methyl, ethyl, propyl) esters, have emerged as viable alternatives to petroleum-based fuels. From a combustion chemistry standpoint, there is great interest in developing accurate reaction models for these new molecules that can be used to predict their behaviors in various regimes. In this paper, we report a detailed study of the unimolecular decomposition pathways of methyl butanoate (MB), a short-chain ester that contains the basic chemical structure of biodiesel fuels. Using ab initio/DFT methods, we identified five homolytic fissions of C−C and C−O bonds and five hydrogen transfer reactions. Rate constants were determined using the G3B3 theory coupled with both variational transition state theory and Rice−Ramsperger−Kassel−Marcus/master equation simulations with hindered rotation corrections. Branching ratios in the temperature range 1500−2200 K indicate that the main pathway for thermal decomposition of MB is the reaction $CH_3CH_2CH_2C(=O)OCH_3 \rightarrow C_2H_5 + CH_2C(=O)OCH_3$. The results, in terms of reaction pathways and rate constants, can be used for future development of mechanisms for long alkyl-chain esters.

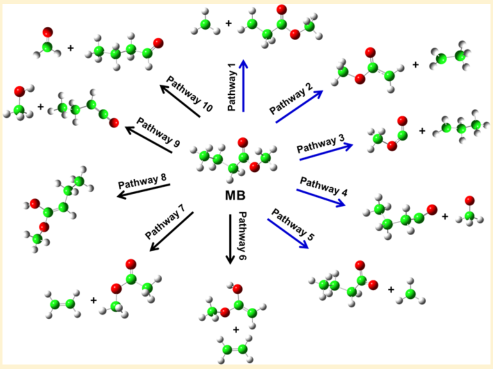

## 1. INTRODUCTION

The use of petroleum-based fuels in the transport sector has raised various societal issues, including air pollution, energy security, and the substantial emission of $CO_2$, which has been linked to climate change.[1] Due to the extensive use of these fuels, researchers are motivated to evaluate alternative solutions. One of the potential alternative fuels that has been suggested is biodiesel, which is typically derived from vegetable oils and animal fats.[2,3] It is composed of a mixture of saturated and unsaturated alkyl esters containing long carbon chains with 16−18 carbon atoms. Such a chemical composition, including the presence of oxygen atoms, introduces new challenges for the development of kinetic mechanisms that describe the behavior of these molecules in combustion conditions.

Methyl butanoate (MB), whose formula is $CH_3CH_2CH_2C(=O)OCH_3$, is a relatively short methyl ester that can be studied computationally to infer the behavior of large biofuel molecules. MB has been chosen as a surrogate for biodiesel, and various theoretical and experimental studies on this molecule have been reported in the literature.[4−20] A recent review by Lai et al.[7] summarizes the research to date on biodiesel molecules, including MB. Our group contributed to this early modeling, creating a submechanism for the reactions of MB radicals using ab initio methods.[13,14] Special emphasis was given to the reactions involving the methoxyformyl radical ($OCOCH_3$), an important intermediate for the formation of $CO_2$ in oxidation conditions. Our results showed very good agreement with the experimental shock tube data for ignition delay obtained by Farooq et al.[16] However, more remains to be done.

Thus, in this follow-up paper, we extend our prior studies to include the unimolecular decomposition pathways of MB, namely C−C or C−O bonds fissions (barrierless reactions) and hydrogen migrations and their corresponding rate constants, using ab initio transition state theory on the basis of the master equation calculation. This study provides a complete picture of the main decomposition pathways of MB, and the results can be used to improve the accuracy and completeness of the MB kinetic mechanism as well as aid in understanding the combustion features of larger biofuels.

## 2. COMPUTATIONAL METHODOLOGY

All electronic structure calculations were carried out using the Gaussian 09 suite of programs.[21] The quantum composite G3B3 method[22] was used to explore the potential energy surfaces (PESs) of each reaction pathway of MB. The G3B3 method is based on geometry optimization, as well as vibrational analysis of molecules, drawing upon the B3LYP/6-31G(d) density functional method.[23,24] This is followed by a series of single-point energy calculations with a higher level of theory QCISDT, MP4, and MP2 with 6-31G(d), 6-31+G(d), 6-31G(2df,p), and G3large basis sets. In addition, G3B3 theory has an empirical correction for spin contamination in open-shell species. Moreover, to improve upon this empirical correction, the spin-unrestricted density functional theory was used, and the G3B3 method was modified by using the option “GUESS=MIX” in the Gaussian calculation. To assess the accuracy of the G3B3 results, we sampled some of the PESs using the more accurate CASSCF(4,4)/6-31G(d) level of theory.[25]

**Received:** March 18, 2013
**Published:** May 16, 2013

For reactions without an intrinsic barrier (barrierless reactions), the variational transition state theory (VTST) was used to determine the PESs.[26−29] Lengths of reacting bonds were varied from 1.5 to 3.5 Å for C−C bonds and 1.45 to 3.5 Å for C−O bonds with intervals of 0.05 Å. For each calculation, we fixed the dissociation bond length and optimized the other geometrical parameters. At each step during the optimization, we carried out a vibrational analysis to obtain the zero-point energy correction.

According to VTST,[30] the rate constant is minimized as a function of reaction coordinate ($s$) and temperature ($T$):

$$k^{\mathrm{VTST}}(T) = \min k^{\mathrm{TST}}(s, T)$$

where $k^{\mathrm{TST}}$ is a rate constant from the transition state theory calculation. The details of the VTST method are discussed in ref 30. For nonbarrierless reactions, minimum energy pathways from reactant to products passing through the transition states were first calculated using the intrinsic reaction coordinate (IRC) method. Once the transition states were located on the PES curve, we used Rice−Ramsperger−Kassel−Marcus/master equation (RRKM/ME) methods to calculate the temperature- and pressure-dependent rate constants using the MESMER code.[31] The temperature-dependent energy transfer relationship, $\langle \Delta E \rangle_{\mathrm{down}} = 200(T/300)^{0.85}$ cm$^{-1}$, was used for our calculations.[32,33] The Lennard-Jones (L-J) parameters for MB ($\sigma$ = 5.55 Å and $\varepsilon/k_B$ = 586 K) used in our calculations were based on the Tee−Gotoh−Steward correlation model.[34] The $N_2$ bath gas L-J parameters ($\sigma$ = 3.74 Å and $\varepsilon/k_B$ = 82 K) were taken from literature.[35]

The one-dimensional (1-D) hindered rotation potentials of the $CH_3$, $C_2H_5$, and $C_3H_7$ (along the C−C bond) and $OCH_3$ and $CH_3$ (along the C−O bond) groups were obtained using the B3LYP/6-31G(d) level of theory. In order to assess their contributions, the vibrational modes, rotating groups, and periodicity number of torsional potential were identified. The 1-D torsional PESs of 12C−10C, 10C−8C, 8C−1C, 1C−3O, and 3O−4C bonds in both MB and transition states (elongated C−C and C−O bonds of MB) of barrierless pathways 1−5 were computed by fixing the dihedral angle for a given rotation (refer to Figure 1 for atom numbers). The minimum energy structure was computed using a constrained optimization routine. The resulting potential was fitted to a Fourier cosine expansion using the approach developed by J. D. Lewis as implemented in the MESMER code.[31] For the transition state calculations of nonbarrierless reactions, rigid rotor harmonic oscillator assumptions were used for all the vibrational modes.

Entropy contributions of each reaction pathway were computed using the partition functions determined at the G3B3 level of theory. The bond dissociation energies (BDEs) were computed using the methodology reported by Blanksby and Ellison,[36] which was developed for systems of unimolecular reactions that lack a well-defined transition state.

## 3. RESULTS AND DISCUSSION

Using the G3B3 method, we optimized the gauche and staggered conformations of MB and identified a difference of 0.1 kcal mol$^{-1}$ between them due to the additional weak interaction that exists between atoms 2O and 15H (Figure 1). In this section, we report an analysis of the decomposition pathways of the gauche conformer of MB.

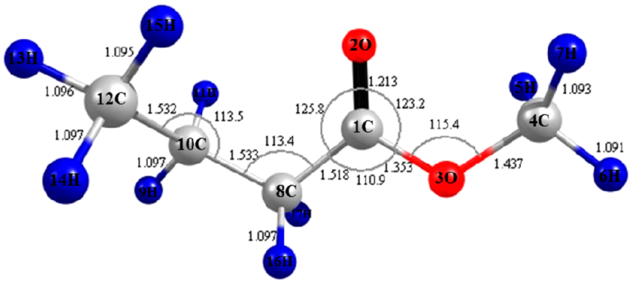

**Figure 1.** Optimized geometry of MB at the B3LYP/6-31G(d) level of theory.

In high temperature regimes, MB can undergo C−C and C−O bond fissions or through hydrogen migration with simultaneous bonds breaking and forming. Figure 2 reports 10 different reaction pathways identified for the unimolecular thermal decomposition of MB. Pathways 1−5 depict homolytic C−C and C−O bond fissions (barrierless reactions), leading to the formation of two radicals. These reaction pathways involve the formation of singlet diradical transition states. Pathways 6−10 show five hydrogen transfer reaction pathways. Sections 3.1 and 3.2 report the details of these pathways. Section 3.3 describes the results for rate constants and branching ratios for pathways 1−10, highlighting the relative importance of the decomposition pathways of MB.

### 3.1. Decomposition Reaction Pathways 1−5: Barrierless.

Pathways 1−5 include three homolytic C−C bond (10C−12C, 10C−8C, and 8C−1C) and two homolytic C−O bond (1C−3O and 3O−4C) fissions. The BDEs of these pathways, computed using the methodology of Blanksby and Ellison[36] as mentioned in the previous section, are shown in Table 1. This table presents the BDE of each bond in MB, namely 12C−8C, 10C−8C, 8C−1C, 1C−3O, and 3O−4C, and the range of the barrier heights of pathways 1−5 at the G3B3 level of theory in the temperature range 800−2200 K. In all cases, the values of the BDEs are higher than the barrier heights because for a given dissociation, the transition state is located at a bond length shorter than that of the fully dissociated products.

The weakest bond in MB is the CC−CC(O)OC bond, and the CCCC(O)−OC bond is the strongest. El-Nahas et al.[9] calculated the BDEs for MB at the CBS-QB3 level of theory, and their results are also reported in Table 1, showing good agreement with our data. Experimentally reported values of BDEs for the dissociation of $CH_3$, $C_2H_5$, and $C_3H_7$ from various alkanes are also similar to our results.[37] These comparisons provide extra credibility to our G3B3 calculations.

*3.1.1. Potential Energy Surfaces.* The potential energy surfaces of reaction pathways 1−5 are shown in Figure 3. The transition states separate a reactant region from a complex region with short fragment separations with a delicate balance between the entropic and enthalpic contribution to the motions of the fragments. The absence of a barrier leads to a weak dependence on the enthalpic factor and a corresponding strong dependence on the entropic factor. Entropy decreases as the fragments get together, as the free rotors become hindered rotors, and eventually bends vibrations. In addition, the coupling between the translational modes and the reaction coordinates varies strongly with separation.

For the five pathways, the transition states are located in the range of bond lengths 2.6−3.5 Å (Table 1 and Figure 3). Pathway 2 has the lowest values of energy due to a resonance effect among the unpaired electron on the 8C and C═O bond. Pathway 1 has the second-lowest energy among the five pathways considered, with the energies of the transition states in the range of 75.4−83.4 kcal mol$^{-1}$. Because 1C is a carbonyl carbon atom, the PES of pathway 3 is the highest among the pathways of C−C bond dissociations. The energies of the transition states are between 83.0 and 89.3 kcal mol$^{-1}$. Pathway 4 describes the dissociation of the carbonyl carbon (CO−O) bond; it has the highest PES among all the dissociation pathways. The energies of the transition states of pathway 4 lie

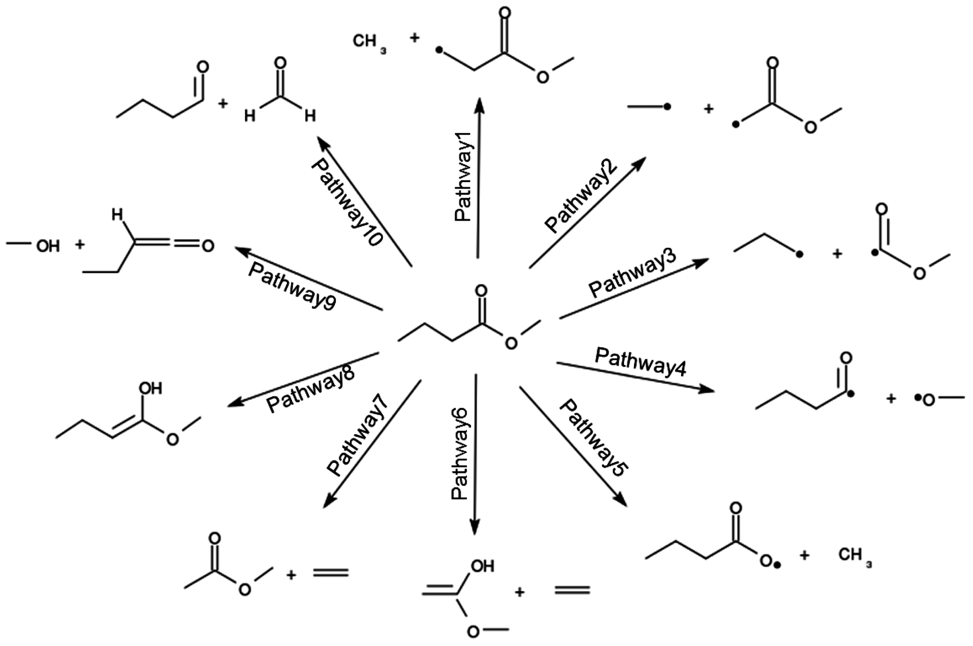

**Figure 2.** The 10 reaction pathways for the unimolecular decomposition of MB considered in this study.

**Table 1. Comparison between the Calculated Reaction Barriers (kcal mol$^{-1}$) in the Temperature Range 800−2200 K and the Bond Dissociation Energies at 0 K (kcal mol$^{-1}$) for Pathways 1−5**

| pathway | barrier height | BDE | BDE[9] |
|---|---|---|---|
| 1 | 83.4−75.4 | 87.1 | 89.1 |
| 2 | 79.3−74.8 | 84.1 | 84.4 |
| 3 | 89.3−83.0 | 93.6 | 93.4 |
| 4 | 97.4−94.8 | 100.4 | 101.3 |
| 5 | 86.7−83.7 | 86.3 | 87.0 |

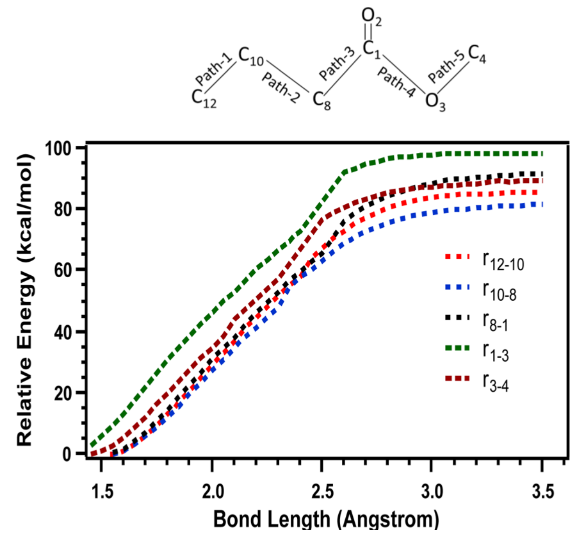

**Figure 3.** Potential energy surfaces of reaction pathways 1−5 at the G3B3 level of theory.

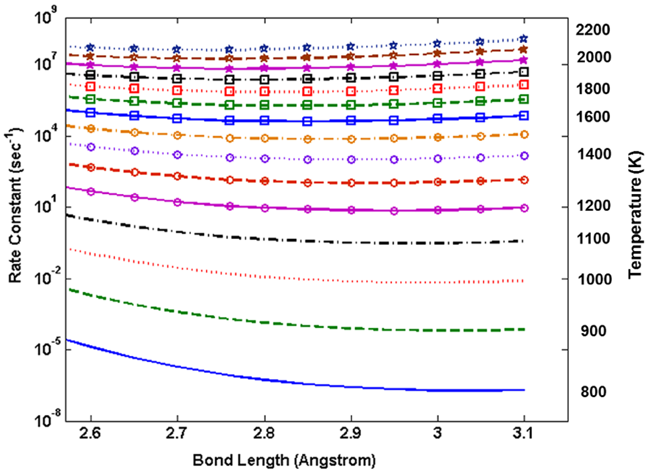

**Figure 4.** Calculated rate constants of pathway 2 at the G3B3 level of theory as a function of the distance $r_{10-8}$ between 8C and 10C in the MB structure, computed in the temperature range 800−2200 K.

in the range 94.8−97.4 kcal mol$^{-1}$ on the PES. Even though pathway 5 involves the breaking of a C−O bond, its PES has a lower energy than pathway 4; this is due to the high electron density on the 1C atom compared to that of the 4C atom. The transition states of pathway 5 are located in the region of 83.7−86.7 kcal mol$^{-1}$. In the case of pathways 4 and 5, the C−O bond dissociations lead to the formation of $CH_3CH_2CH_2C(=O)O$ and $OCH_3$ radicals, which may have several degenerate electronic states. The low-lying electronic states of these radicals are not the focus of this study, so we used the ground electronic state of these radicals.[33]

To gain more confidence in the performance of the G3B3 method, the results of some of these pathways were also verified with the multireference CASSCF(4,4)/6-31G(d) method. As an example, Figure S1 (Supporting Information) shows the comparison between the values of PESs obtained with the two methods for pathway 2. The results for the values of the reaction coordinates in the range 2.55−3.40 Å are very similar, supporting that the use of the G3B3 method in the region where the transition states are located is appropriate.

*3.1.2. Location of Transition States.* At each point on the PES (from 2.6 to 3.5 Å), we computed the rate constants as functions of bond length, namely $r_{12-10}$, $r_{10-8}$, $r_{8-1}$, $r_{1-3}$, and

Table 2. Bond Lengths of Transition States and Calculated Barrier Heights at the G3B3 Level of Theory for Reaction Pathways 1−5 at Different Temperatures

| | | | | | | |
|---|---|---|---|---|---|---|
| a. Pathway 1 | | | | | | |
| temperature | 800−1100 K | 1200−1300 K | 1400−1500 K | 1600−1700 K | 1800−2100 K | 2200 K |
| bond length (Å) | 2.95 | 2.85 | 2.80 | 2.75 | 2.70 | 2.65 |
| energy (kcal $mol^{-1}$) | 83.4 | 81.8 | 80.6 | 79.2 | 77.5 | 75.4 |
| b. Pathway 2 | | | | | | |
| temperature | 800−1000 K | 1100−1300 K | 1400−1500 K | 1600−1700 K | 1800−1900 K | 2000−2200 K |
| bond length (Å) | 3.00 | 2.95 | 2.90 | 2.85 | 2.80 | 2.75 |
| energy (kcal $mol^{-1}$) | 79.3 | 78.6 | 77.9 | 77.0 | 75.9 | 74.8 |
| c. Pathway 3 | | | | | | |
| temperature | 800−1600 K | 1700 K | 1800−2100 K | 2200 K | | |
| bond length (Å) | 3.05 | 2.95 | 2.85 | 2.75 | | |
| energy (kcal $mol^{-1}$) | 89.3 | 87.9 | 85.6 | 83.0 | | |
| d. Pathway 4 | | | | | | |
| temperature | 800 K | 900−1000 K | 1100−1300 K | 1400−1600 K | 1700−2200 K | |
| bond length (Å) | 2.90 | 2.85 | 2.80 | 2.75 | 2.70 | |
| energy (kcal $mol^{-1}$) | 97.4 | 97.0 | 96.5 | 95.8 | 94.8 | |
| e. Pathway 5 | | | | | | |
| temperature | 800 K | 900−1000 K | 1100−1300 K | 1400 K | 1500−2200 K | |
| bond length (Å) | 2.90 | 2.85 | 2.80 | 2.75 | 2.70 | |
| energy (kcal $mol^{-1}$) | 86.7 | 86.2 | 85.5 | 84.6 | 83.7 | |

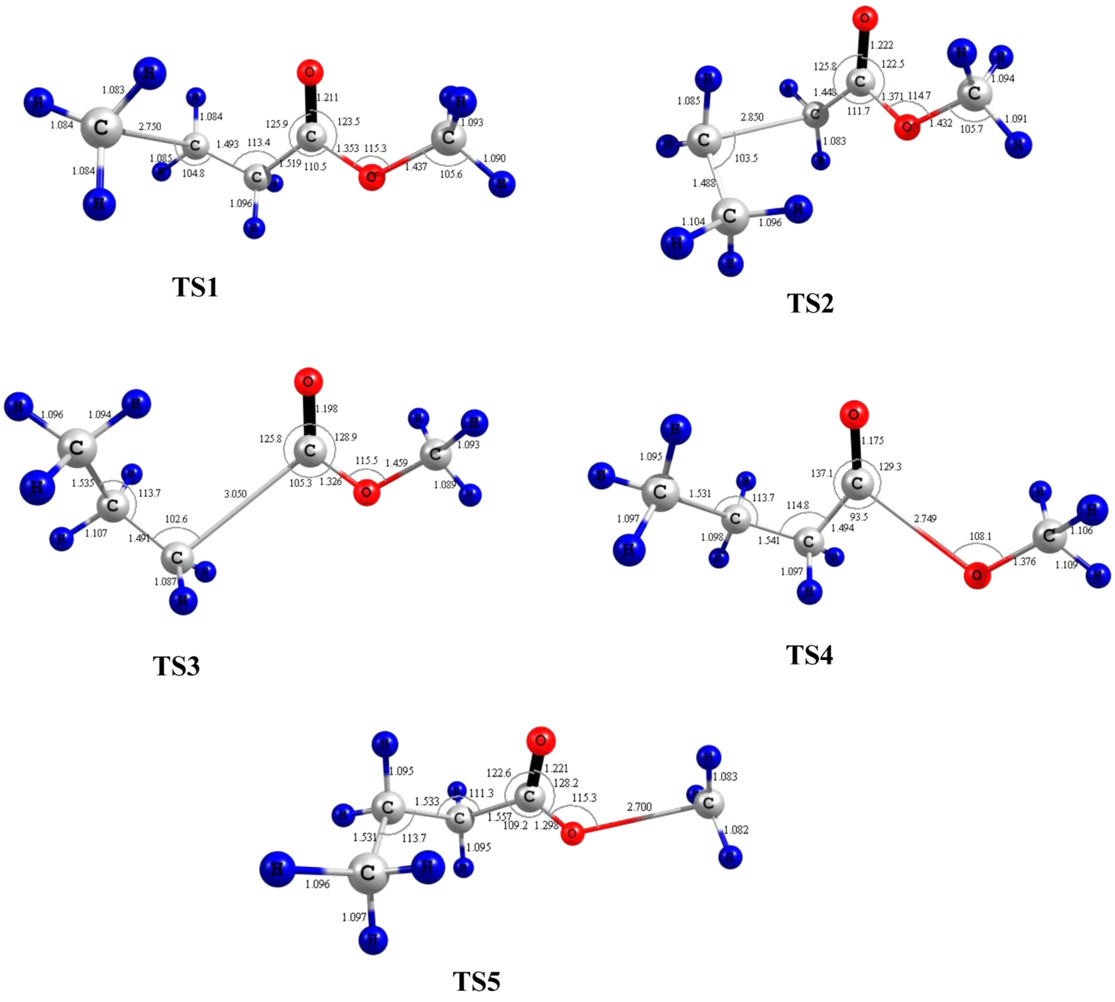

**Figure 5.** Optimized geometries of the transition states of pathways 1−5 at the uB3LYP/6-31G(d) level of theory at 1600 K.

$r_{3-4}$, in the temperature range 800−2200 K. The calculated rate constants of reaction pathway 2 as a function of $r_{10-8}$ in the temperature range 800−2200 K are given in Figure 4. This figure shows that, at low temperatures, the rate constant decreases with bond length, and it remains unchanged at longer bond lengths. At high temperatures, the rate constant decreases

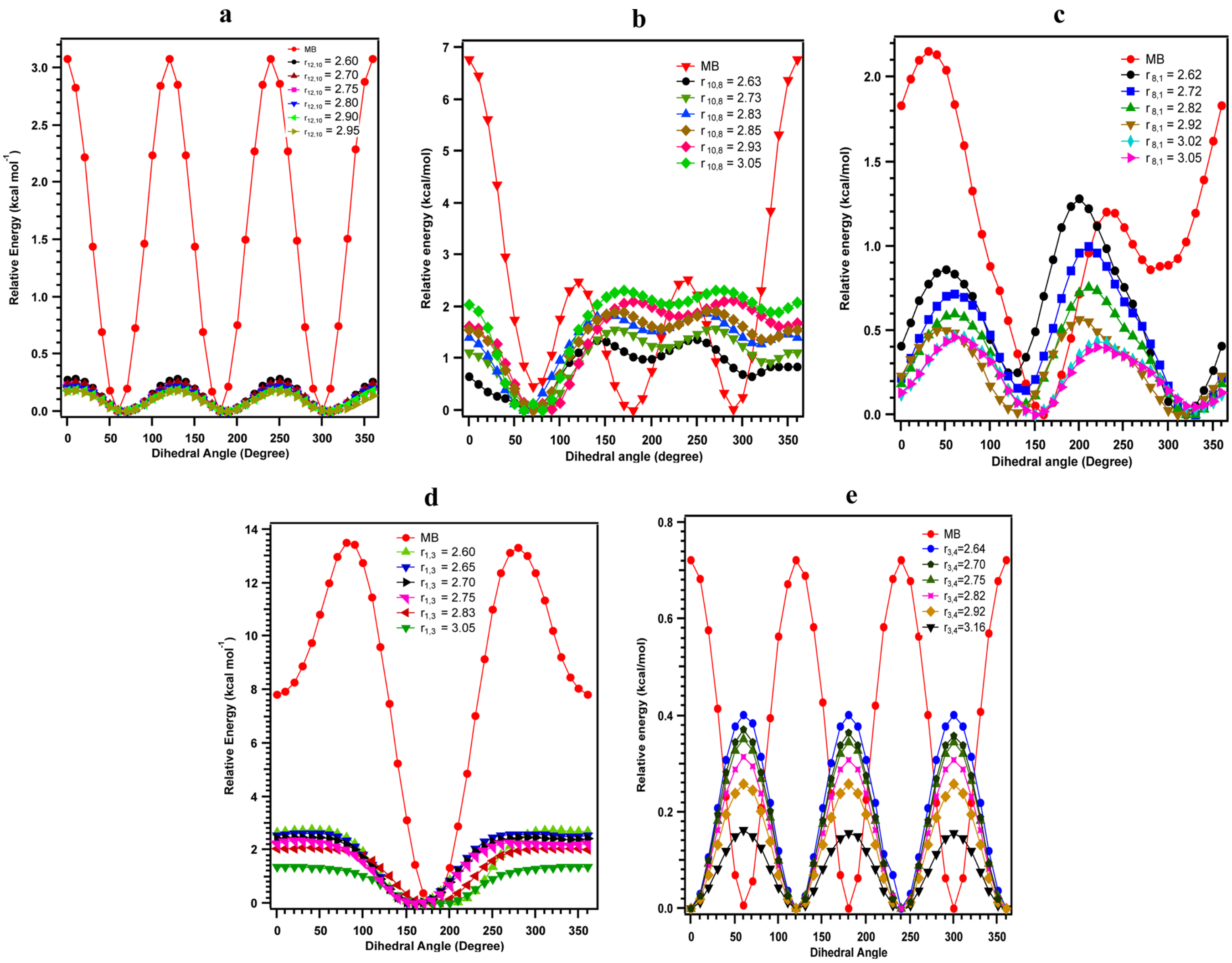

**Figure 6.** Torsional potential energy surfaces for the bonds 12C−10C, 10C−8C, 8C−1C, 1C−3O, and 3O−4C in the MB structure, computed at the B3LYP/631G(d) level of theory.

### Table 3. Rotational Barriers of C−C and C−O Single Bonds from 0° to 360° of MB and Transition States at the B3LYP/6-31G(d) Level of Theory

| bond | torsional potential of MB (kcal mol$^{-1}$) | torsional potential of transition states (kcal mol$^{-1}$) |
|---|---|---|
| 12C−10C | 3.08 | 0.28−0.17 ($r_{10-12}$ = 2.60−2.95 Å) |
| 10C−8C | 2.96 | 1.34−2.31 ($r_{8-10}$ = 2.63−3.05 Å) |
| | 6.76 | 0.84−2.04 ($r_{8-10}$ = 2.63−3.05 Å) |
| 8C−1C | 2.15 and 1.19 | 0.13−1.28 ($r_{1-8}$ = 2.63−3.05 Å) |
| 1C−3O | 5.66 and 13.49 | 2.64−1.35 ($r_{1-3}$ = 2.60−3.05 Å) |
| 3O−4C | 0.72 | 0.40−0.15 ($r_{3-4}$ = 2.60−3.05 Å) |

with bond length and increases at longer bond lengths. This result is due to the entropic contribution, which becomes more relevant as temperature increases. A similar trend was observed for the other four pathways (1, 3−5), and the results are reported in Figure S2 (Supporting Information). Table 2 reports the reaction barrier heights at different reaction temperatures for pathways 1−5. Once the transition states were located on the PES profile, we used the optimized geometries of these transition states in our rate constant calculations. All the transition states of pathways 1−5 shown in Figure 5 have a single imaginary frequency with the vibrational modes corresponding to the C−C and C−O bond cleavages. The normal modes of vibration of these transition states were also verified to be consistent with the reaction of interest through visualization with GaussView.[38]

*3.1.3. Hindered Rotation Potential.* To account for quantum mechanical hindered rotor corrections in the rate constant calculations, we computed 1-D hindrance potentials of MB and the relevant transition states at the B3LYP/6-31G(d) level of theory. The results are reported in Figure 6. Both torsional bonds 12C−10C and 3O−4C involve the rotation of a $CH_3$ group, and their torsional potential energy surfaces are found to be similar. The torsional barrier of the 12C−10C bond (3.1 kcal mol$^{-1}$) is higher than the torsional barrier of the 3O−4C bond (0.7 kcal mol$^{-1}$). This result can be ascribed to the electronegativity of the oxygen atom in the 3O−4C bond. The highest torsional barrier (13.5 kcal mol$^{-1}$) is observed in the case of the 1C−3O bond rotation, which is due to the 4C−H interaction with the 2O atom.

Table 3 summarizes the rotational barriers of MB and the transition states. Because the C−C and C−O bond lengths at the transition states are longer than the corresponding bonds in MB, the rotational barriers of the transition states are lower than those of MB. In general, when the bond length in the transition state increases, the torsional potential decreases,

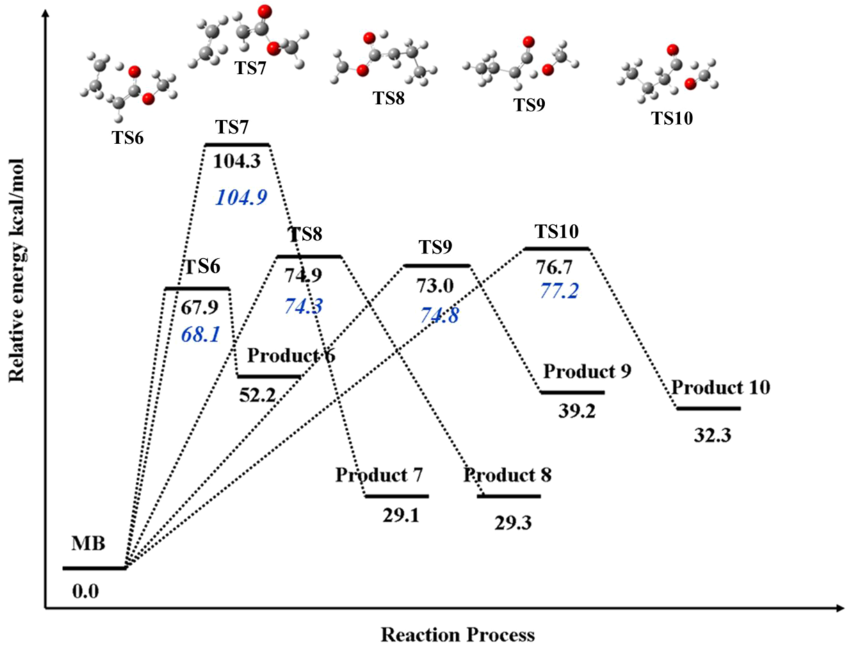

**Figure 7.** Potential energy surfaces of reaction pathways 6−10 computed using the G3B3 level of theory. The data in italics correspond to the study of El-Nahas et al.[9] using the CBS-QB3 method.

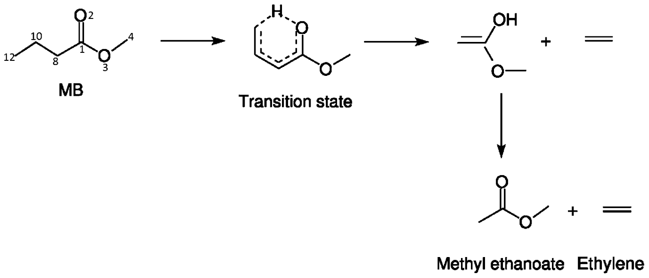

**Figure 8.** Unimolecular decomposition pathways for MB via a six-membered transition state.

except in the case of the 10C−8C bond (pathway 2). Specifically, the torsional barriers of the 10C−8C bond rotation are 6.7 and 2.9 kcal mol$^{-1}$ from the rotation of the 1C−8C−10C−12C dihedral angle. This effect may be due to the increased interaction between 11H and 2O atoms when the transition state bond length decreases.

**3.2. Decomposition Reaction Pathways 6−10.** Figure 7 illustrates the potential energy surfaces for the decomposition reaction labeled as pathways 6−10 computed at the G3B3 level of theory. In the same figure, we also report the barrier heights computed by El-Nahas et al.[9] using the CBS-QB3 method, showing the good agreement between the two sets of data. Pathway 6 proceeds through a hydrogen transfer from 12C to 2O through a six-membered transition state TS6 (Figure 8), leading to the formation of ethylene ($C_2H_4$) and methyl ethanoate ($H_3CC(=O)OCH_3$) through a keto−enol isomerization with a computed barrier height of 67.9 kcal mol$^{-1}$, which is in strong agreement with the values reported earlier in the literature.[6,9,39] In pathway 7, a hydrogen transfer occurs from 12C to 8C via transition state TS7, accompanying the breaking of bond 1C−3O (Figure 9). The barrier height (104.4 kcal mol$^{-1}$) for this reaction is substantially higher compared to those of other pathways. The hydrogen transfers in pathways 8 and 9 via oxygen atoms are more favorable (74.9 and 73.0 kcal mol$^{-1}$, respectively) than the reaction in pathway 10 via the carbon atom (76.7 kcal mol$^{-1}$). This is due to the fact that pathway 8 has only one C−H bond breaking, and pathway 9 has two bonds (C−O and C−H) breaking simultaneously. However, pathway 10 has two bonds (C−O and C−H) breaking and one new C−O bond forming. The optimized geometries of the transition states of pathways 6−10 obtained at the uB3LYP/6-31G(d) level of theory are shown in Figure 9. To confirm that each transition state was connected through the proper reactant and products, we performed intrinsic reaction coordinate (IRC) calculations for pathways 6−10 with 54 steps (in intervals of 0.05 au) at the uB3LYP/6-31G(d) level of theory.

**3.3. Rate Constants.** Using G3B3 potential energy surfaces together with optimized geometries, reactant vibrational frequencies, transition states, and products, the high pressure limit ($k_\infty$) and pressure-dependent rate constants of pathways 1−10 were computed using RRKM/ME coupled with VTST in the temperature range 800−2200 K. Furthermore, the hindered rotor corrections for rotation of $CH_3$, $C_2H_5$, and $C_3H_7$ (along the C−C bond) and $OCH_3$ and $CH_3$ (along the C−O bond) groups of reactant and transition states were accounted for in the rate constant calculations. In addition, branching ratios of each pathway were computed to provide the relative importance of pathways 1−10.

*3.3.1. High Pressure Limit Rate Constants.* Figure 10 shows the computed rate constants of pathways 1−5 in the temperature range 800−2200 K. Rate constants are fitted to a modified Arrhenius equation, $k(T) = AT^n \exp(-E_a/RT)$, and the parameters are reported in Table 4. Among all the homolytic bond fissions, pathway 2 has the highest value for the rate constants, and pathway 4 has the lowest value for the rate constants (Figure 10).

Our computed rate constants with a negative temperature dependence are consistent with previous studies for barrierless reactions.[33,40]

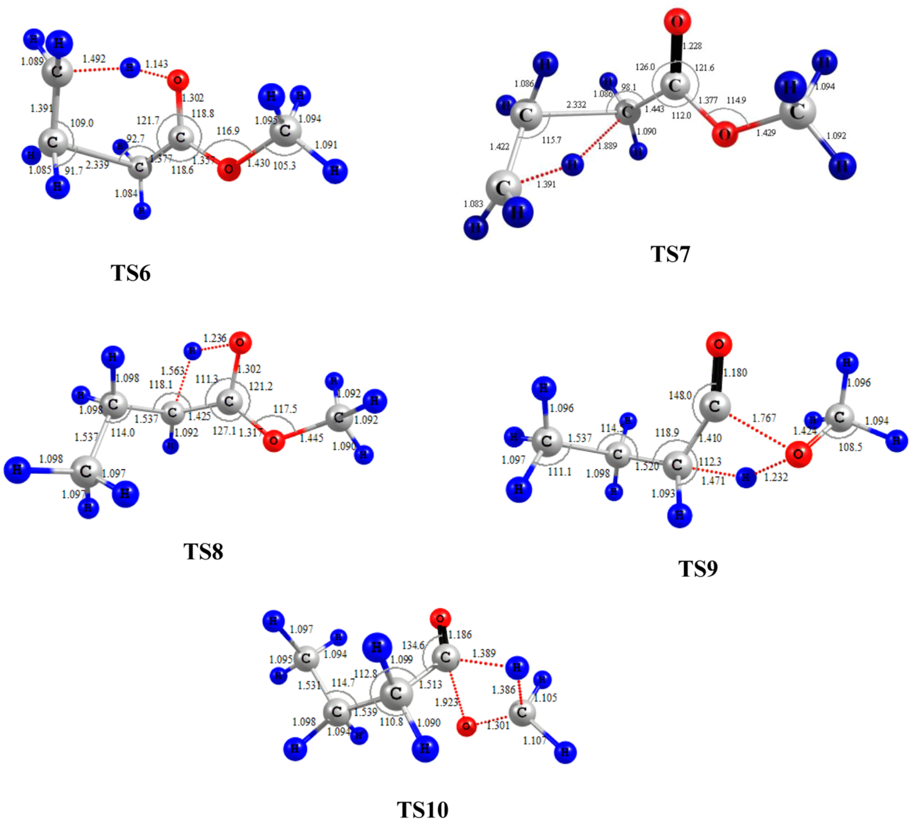

TS6

TS7

TS8

TS9

TS10

**Figure 9.** Optimized geometries of the transition states of pathways 6−10 at the uB3LYP/6-31G(d) level of theory.

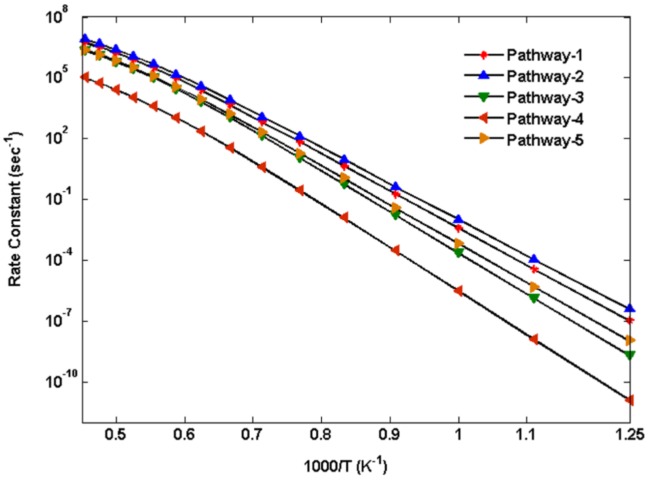

**Figure 10.** Calculated rate constants of pathways 1−5 at the high pressure limit ($k_\infty$).

To validate our results, we compared the rate constants of pathways 1−5 with the values reported of Fisher et al.[4] and Dooley et al.[10] as shown in Figure 11. The rate constants for pathway 1 are in good agreement with previous data by Fisher et al. in the range 900−1200 K and at least one order of magnitude slower at high temperatures. The data of Dooley et al.[10] match our new computed values very well.

Our rate constants for pathways 2 and 3 are in good agreement with the values of Fisher et al.[4] in the temperature range 1100−2200 K (Figure 11). However, at least one order of magnitude difference is observed in the temperature range 800−1000 K. The discrepancy in rate constants for pathways 4 and 5 is found at low temperatures. The agreement at high temperatures, however, is very positive.

The rate constants of pathways 2−5 of Dooley et al.[10] are one order magnitude higher than our results in the entire temperature range.

To further validate our G3B3 results, we compared the dissociation rate constant of $CH_3$ present in pathway 1 with available data in the literature.[41] Our computed rate constants [$5.41 \times 10^{15}\ T^{-0.197} \exp(-40273/T)\ \text{s}^{-1}$] are similar to the rate constants reported for the elimination of $CH_3$ from $CH_3CONH_2$ [$(2.54 \times 10^{12}\ T^{0.92} \exp(-40100/T)\ \text{s}^{-1}$] obtained using the G3MP2B3 level of theory,[41] as well as with values reported for the elimination of $CH_3$ from $CH_3CHO$ [$6.0 \times 10^{14} \exp(-39808/T)$].[42] Our computed rate constants are in good agreement with the reported rate constants for the elimination of $CH_3$ [$2.5 \times 10^{16} \exp(-42410/T)\ \text{s}^{-1}$] and $C_2H_5$ [$2.5 \times 10^{16}$

**Table 4. Arrhenius Parameters of Rate Constants for the Unimolecular Decomposition Pathways of MB at the High Pressure Limit**

| pathway | $A$ | $n$ | $E_a$ (kcal mol$^{-1}$) |
|---|---|---|---|
| 1 | $5.41 \times 10^{15}$ | −0.1970 | 80.0 |
| 2 | $4.03 \times 10^{15}$ | −0.1844 | 77.7 |
| 3 | $2.15 \times 10^{16}$ | −0.2462 | 87.6 |
| 4 | $4.30 \times 10^{15}$ | −0.2829 | 92.5 |
| 5 | $6.58 \times 10^{15}$ | −0.2180 | 83.6 |
| 6 | $2.67 \times 10^{13}$ | −0.1313 | 68.6 |
| 7 | $1.99 \times 10^{14}$ | −0.3346 | 99.6 |
| 8 | $2.15 \times 10^{13}$ | −0.1618 | 73.9 |
| 9 | $1.66 \times 10^{14}$ | −0.1570 | 73.0 |
| 10 | $1.09 \times 10^{13}$ | −0.1711 | 75.4 |

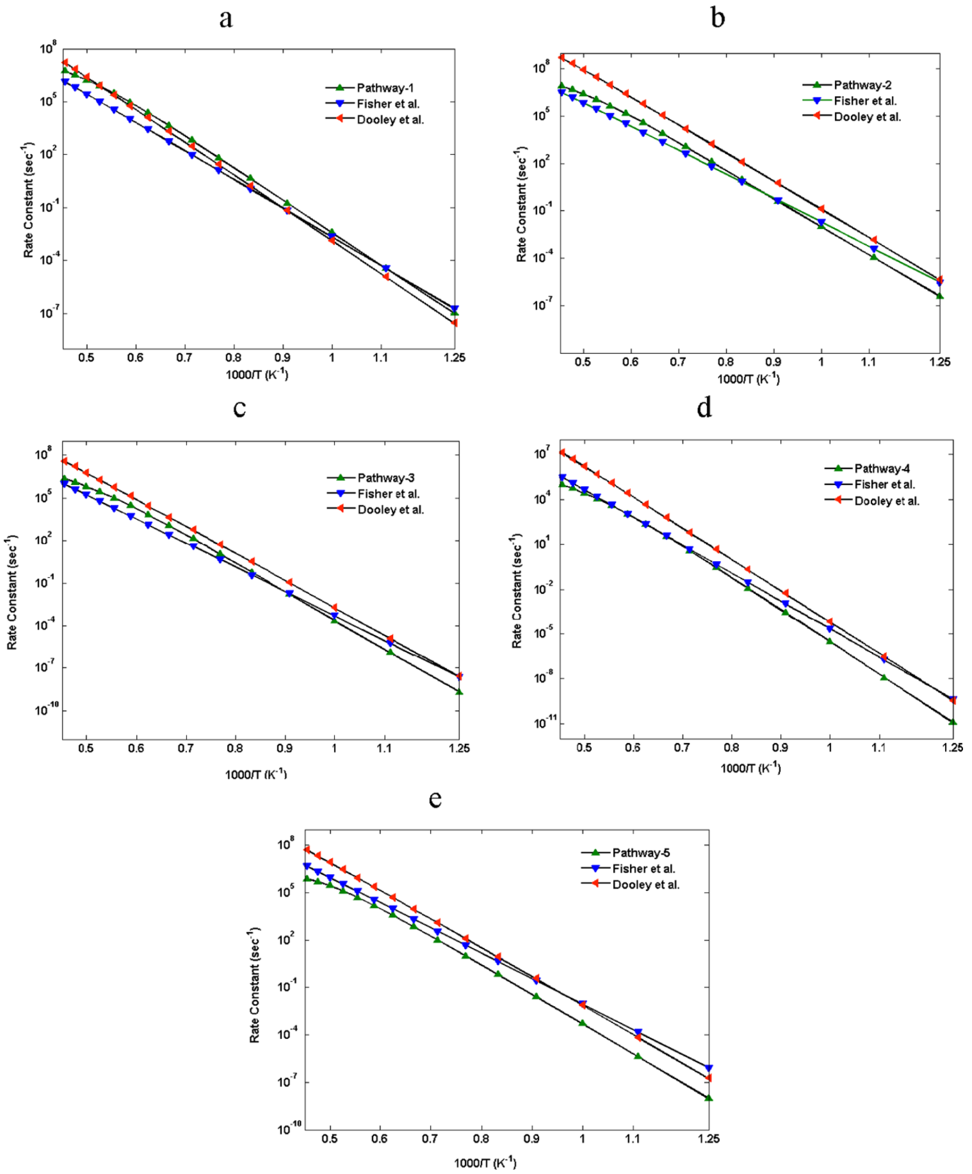

**Figure 11.** Comparison between the newly computed rate constants for pathways 1−5 and the data of Fisher et al.[4] and Dooley et al.[10]

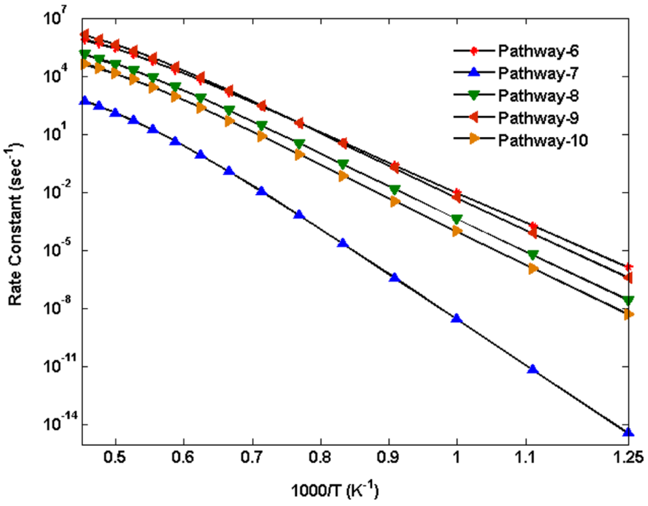

**Figure 12.** Calculated rate constants of pathways 6−10 at the high pressure limit ($k_\infty$).

**Table 5. Standard Entropy, Entropy of Activation (cal mol$^{-1}$ K$^{-1}$), and Barrier Heights (kcal mol$^{-1}$) for Reaction Pathways 1−10 at the G3B3 Level of Theory**

| pathway | $S^0_{298}$ of TS | $\Delta S^{\ddagger}_{298}$ |
|---|---|---|
| 1 | 96.9 | 6.1 |
| 2 | 96.9 | 6.1 |
| 3 | 95.4 | 4.6 |
| 4 | 100.5 | 9.7 |
| 5 | 98.1 | 7.3 |
| 6 | 87.5 | −3.3 |
| 7 | 94.3 | 3.5 |
| 8 | 89.1 | −1.7 |
| 9 | 92.1 | 1.3 |
| 10 | 87.8 | −3.1 |

exp(−41150/$T$) s$^{-1}$] from $n$-butanol in the temperature range 800−1200 K.[43] However, our rate constants are slower by a factor of 4 in the temperature range 1300−2200 K. We have also compared our rate constant for elimination of $C_2H_5$ from $n$-propane [$(1.29 \times 10^{37}\ T^{-5.84}\ \exp(-49010/T)\ s^{-1}$].[44] The rate

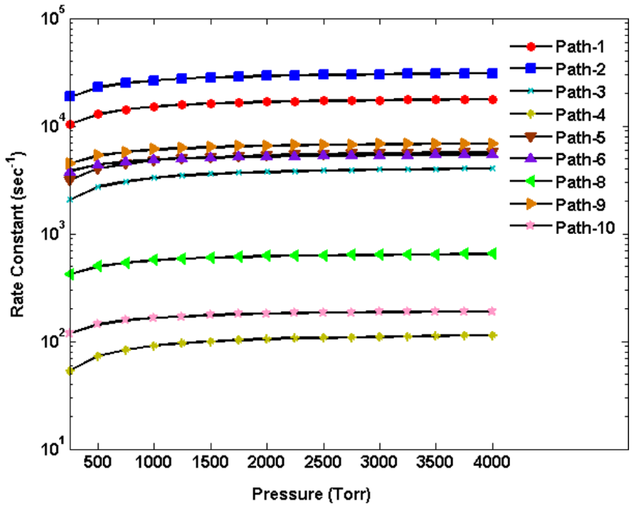

**Figure 13.** Calculated rate constants in the falloff regions for the unimolecular decomposition pathways of MB at 1600 K.

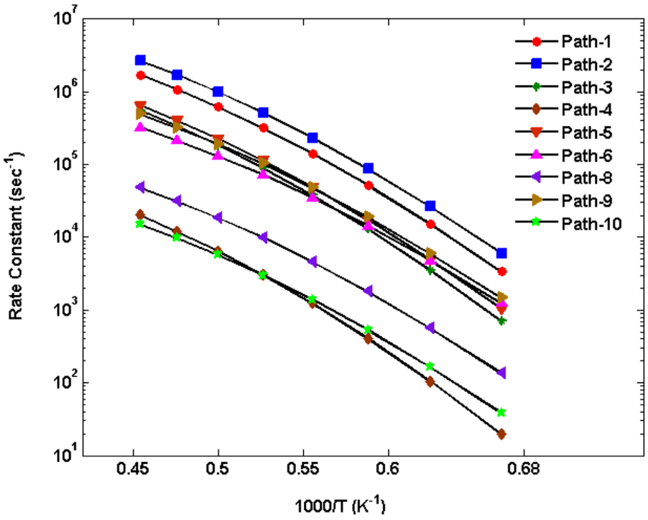

**Figure 14.** Temperature-dependent rate constants at 760 Torr.

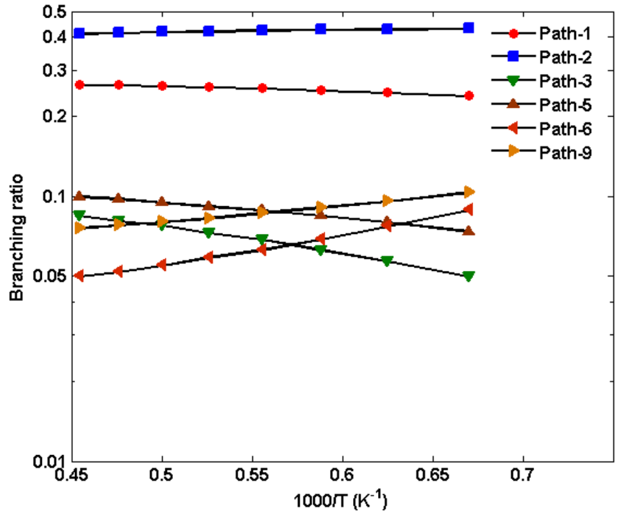

**Figure 15.** Temperature-dependent branching ratio of the unimolecular decomposition reaction of MB at 760 Torr.

constants are in good agreement with our value for pathway 2 in the temperature range 900−1200 K (Table 4).

Figure 12 shows the computed rate constants of pathways 6−10 at the high pressure limit $k_\infty$ using RRKM/ME in the temperature range 800−2200 K. Among all the hydrogen migration channels, pathways 6 and 9 have the highest values for rate constants, and pathway 7 has the lowest value. In the case of pathway 6, formation of ethylene via a six-membered transition state is favorable both thermodynamically and kinetically in the low temperature regimes. At higher temperatures, the formation of methanol (pathway 9) is kinetically more favorable. This result is consistent with previous studies by Gail et al.,[5] Sarathy et al.,[12] and Dooley et al.[10] To further validate our results, we compared the rate constant for pathway 6 (Table 4) with available rate constants in the literature.[6] The rate constant in our calculation [$2.7 \times 10^{13}\ T^{-0.1313}\ \exp(-68600/RT)\ \mathrm{s}^{-1}$] is in strong agreement with the rate constant [$4.0 \times 10^{12}\ \exp(-68000/RT)\ \mathrm{s}^{-1}$] reported by Metcalfe et al.[6]

As mentioned in Computational Methodology, to understand the entropy contribution in the rate constant calculations, the standard entropy of reactant, transition states, and products of each pathway involved in decomposition of MB were computed using the G3B3 level of theory. The standard entropy of transition states and entropy of activation (entropy difference between transition state and reactant) of pathways 1−10 are listed in Table 5. Pathways 1−5 have higher values of entropy of activation than pathways 6−10, which can be ascribed to the fact that homolytic bond fission is entropically more favorable than hydrogen migration, and this has a substantial effect on rate constant calculations. The decrease in reaction rate constants in the case of pathways 6, 8, and 10, when compared to those of pathways 1−3 and 9, is due to the increasingly negative value of entropy change $\Delta S^{\ddagger}$. Our calculations report the importance of the entropy contribution on the decomposition pathways of MB differently than previous published work.[9]

*3.3.2. Pressure-Dependent Rate Constants.* Figure 13 reports the rate constants in the falloff regions for the decomposition pathways at 1600 K. The values of rate constants for pathway 7 are negligible compared with those of the other pathways, and therefore they are not reported in the figure. The calculated rate constants (temperature dependent) at 760 Torr obtained in the temperature range 1500−2200 K are shown in Figure 14. Among all the systems that were studied, pathways 1, 2, 5, and 9 present the highest rate constants and pathways 4, 8, and 10 have the lowest rate constants. A complete list of calculated rate constants as a function of pressure for all the reaction pathways at 0.01, 0.1, 0.2, and 1 atm is included in the Supporting Information.

To provide insights into the relative importance of these pathways, we determined the branching ratios for pathways 1−10 in the temperature range 1500−2200 K at 760 Torr. The results are reported in Figure 15. The values for pathways 7, 8, and 10 are minor compared to the values of the others routes. Pathway 2 contributes 43−44%, and pathway 1 contributes 24−26% in the temperature range 1500−2200 K, which is consistent with previous studies.[10] The third most important pathway is the production of methanol ($CH_3OH$) and ethyl ketene ($CH_3CH_2HC{=}C({=}O)$) (pathway 9) in the temperature range 1500−1800 K, and methyl ($CH_3$) and $CH_3CH_2CH_2C({=}O)O$ radicals (pathway 5) in the temperature range 1900−2200 K.

## 4. CONCLUSION

This work reports on a detailed analysis of the unimolecular decomposition pathways of methyl butanoate, using ab initio/DFT methods. The network of reactions includes carbon−carbon and carbon−oxygen bond cleavage (barrierless reactions) and hydrogen transfer pathways. Our results provide a comprehensive picture of the unimolecular decomposition pathways of MB that include an analysis of homolytic bond fissions and hydrogen transfers together with insights into the pressure-dependent rate constants and branching fractions for these pathways. Pathways 1, 4, 8, and 10 are novel.

All the structures and related molecular properties of each species involved in the decomposition reaction pathways were explored using the high-level quantum composite G3B3 method. The rate constants were calculated using the G3B3 level of theory coupled with VTST and the RRKM/ME method with hindered rotor corrections in the temperature range 800−2200 K.

This study also highlights, for the first time, the importance of entropic contributions during the unimolecular decomposition of MB. The rate constants and branching ratios in different temperature ranges indicate that the main reaction pathway for thermal decomposition of MB is the $CH_3CH_2CH_2C(=O)OCH_3 \rightarrow C_2H_5 + CH_2C(=O)OCH_3$, with a smaller contribution from the hydrogen migration channels.

Such results for short-chain methyl esters are encouraging, and the kinetic parameters of the new mechanisms can be used as a basis for future implementation of longer alkyl-chain ester biodiesels.

## ■ ASSOCIATED CONTENT

### Ⓢ Supporting Information

Tables of optimized geometries and vibrational frequencies of reactants, transition states, and products at the B3LYP/6-31G(d) level of theory; tables of the G3B3 energies of reactants, transition states, and products for important species; plots of rate constants versus reaction coordinates for pathways 1, 3, 4, and 5; comparison of PES of reaction pathway 2 at the G3B3 and CASSCF(4,4)/6-31G(d) levels of theory; and tables of pressure-dependent (0.01, 0.1, 0.2, and 1 atm) rate constants in the temperature range 800−2200 K. This material is available free of charge via the Internet at http://pubs.acs.org.

## ■ AUTHOR INFORMATION

### Corresponding Author

*E-mail: avioli@umich.edu.

### Notes

The authors declare no competing financial interest.

## ■ ACKNOWLEDGMENTS

M.A.A. thanks Jason Lai for the helpful discussions and suggestions. This material is based upon work supported by the Department of Energy under Award DE-PI0000012.

## ■ REFERENCES

(1) Solomon, S.; Qin, D.; Manning, M.; Chen, Z.; Marquis, M.; Averyt, K. *IPCC Fourth Assessment Report*; Tignor, M., Miller, H. L., Eds.; Cambridge University Press: Cambridge, U.K., 2007.

(2) Graboski, M. S.; McCormick, R. L. *Prog. Energy Combust. Sci.* **1998**, *24*, 125−164.

(3) Bozbas, K. *Renewable Sustainable Energy Rev.* **2008**, *12*, 542−552.

(4) Fisher, E. M.; Pitz, W. J.; Curran, H. J.; Westbrook, C. K. *Proc. Combust. Inst.* **2000**, *28*, 1579−1586.

(5) Gail, S.; Thomson, M. J.; Sarathy, S. M.; Syed, S. A.; Daguat, P.; Dievart, P.; Marchese, A. J.; Dryer, F. L. *Proc. Combust. Inst.* **2007**, *31*, 305−311.

(6) Metcalfe, W. K.; Dooley, S.; Curran, H. J.; Simmie, J. M.; El-Nahas, A. M.; Navarro, M. V. *J. Phys. Chem. A* **2007**, *111*, 4001−4014.

(7) Lai, J. Y. W.; Lin, K. C.; Violi, A. *Prog. Energy Combust. Sci.* **2011**, *37*, 1−14.

(8) Walton, S. M.; Karwat, D. M.; Teini, P. D.; Gorny, A. M.; Wooldridge, M. S. *Fuel* **2011**, *90*, 1796−1804.

(9) El-Nahas, A. M.; Navarro, M. V.; Simmie, J. M.; Bozzelli, J. W.; Curran, H. J.; Dooley, S.; Metcalfe, W. *J. Phys. Chem. A* **2007**, *111*, 3727−3739.

(10) Dooley, S.; Curran, H. J.; Simmie, J. M. *Combust. Flame* **2008**, *153*, 2−32.

(11) Gail, S.; Sarathy, S. M.; Thomson, M. J.; Diévart, P.; Dagaut, P. *Combust. Flame* **2008**, *155*, 635−650.

(12) Sarathy, S. M.; Gail, S.; Syed, S. A.; Thomson, M. J.; Dagaut, P. *Proc. Combust. Inst.* **2007**, *31*, 1015−1022.

(13) Huynh, L. K.; Lin, K. C.; Violi, A. *J. Phys. Chem. A* **2008**, *112*, 13470−13480.

(14) Huynh, L. K.; Violi, A. *J. Org. Chem.* **2008**, *73*, 94−101.

(15) Herbinet, O.; Pitz, W. J.; Westbrook, C. K. *Combust. Flame* **2008**, *154*, 507−528.

(16) Farooq, A. D.; Davidson, F.; Hanson, R. K.; Huynh, L. K.; Violi, A. *Proc. Combust. Inst.* **2009**, *32*, 247−253.

(17) Hakka, M. H.; Bennadji, H.; Biet, J.; Yahyaoui, M.; Sirjean, B.; Warth, V. *Int. J. Chem. Kinet.* **2010**, *42*, 226−252.

(18) Akih-Kumgeh, B.; Bergthorson, J. M. *Energy Fuels* **2010**, *24*, 2439−2448.

(19) Yang, B.; Westbrook, C. K.; Cool, T. A.; Hansen, N.; Kohse-Hoinghaus, K. *Phys. Chem. Chem. Phys.* **2011**, *13*, 6901−6913.

(20) Westbrook, C. K.; Naik, C. V.; Herbinet, O.; Pitz, W. J.; Mehl, M.; Sarathy, S. M. *Combust. Flame* **2011**, *158*, 742−755.

(21) Frisch, M. J.; et al. *Gaussian 09*, revision A.1; Gaussian, Inc.: Wallingford, CT, 2009.

(22) Baboul, A. G.; Curtiss, L. A.; Redfern, P. C.; Raghavachari, K. *J. Chem. Phys.* **1999**, *110*, 7650−7657.

(23) Becke, A. D. *J. Chem. Phys.* **1993**, *98*, 5648−5652.

(24) Francl, M. M.; Pietro, W. J.; Binkley, J. S.; Gordan, M. S.; Defrees, D. J.; Pople, J. A. *J. Chem. Phys.* **1982**, *77*, 3654−3665.

(25) Andersson, K.; Malmqvist, P.-A.; Roos, B. O. *J. Phys. Chem.* **1990**, *94*, 5483−5488.

(26) Klippenstein, S. J.; Harding, L. B. *J. Phys. Chem. A* **1999**, *103*, 9388−9398.

(27) Mousavipour, S. H.; Emad, L.; Fakhraee, S. *J. Phys. Chem. A* **2002**, *106*, 2489−2496.

(28) da Silva, G.; Bozzelli, J. W. *J. Phys. Chem. A* **2008**, *112*, 3566−3575.

(29) da Silva, G.; Hamdan, M. R.; Bozzelli, J. W. *J. Chem. Theory Comput.* **2009**, *5*, 3185−3194.

(30) Truhlar, D. G.; Garrett, B. C. *Annu. Rev. Phys. Chem.* **1984**, *35*, 159−189.

(31) Robertson, S. H.; Glowacki, D. R.; Liang, C.-H.; Morley, C. M.; Pilling, J.; et al. *MESMER (Master Equation Solver for Multi Energy well Reactions)*; University of Leeds: Leeds, U.K., 2008. http://www.chem.leeds.ac.uk/mesmer.html

(32) Goldsmith, C. F.; Green, W. H.; Klippenstein, S. J. *J. Phys. Chem. A* **2012**, *116*, 3325−3346.

(33) Peukert, S. L.; Sivaramakrishnan, R.; Su, M.-C.; Michael, J. V. *Combust. Flame* **2012**, *159*, 2312−2323.

(34) Wang, Y. L.; Feng, Q.; Egolfopoulos, F. N.; Tsotsis, T. T. *Combust. Flame* **2011**, *158*, 1507−1519.

(35) Hippler, J.; Troe, J.; Wendelken, H. J. *J. Chem. Phys.* **1983**, *78*, 6709−6717.

(36) Blanksby, S. T.; Ellison, G. B. *Acc. Chem. Res.* **2003**, *36*, 255−263.

(37) Alkorta, I.; Elguero, J. *Chem. Phys. Lett.* **2006**, *425*, 221−224.

(38) Nielsen, A.; Holder, A. *GaussView 3.0 User's Reference*; Gaussian, Inc.: Pittsburgh, PA, 2003.
(39) Blades, A. T.; Sandhu, H. S. *Int. J. Chem. Kinet.* **1971**, *3*, 187−193.
(40) Ismail, H.; Abel, P. R.; Green, W. H.; Fahr, A.; Jusinski, L. E.; Knepp, A. M.; Zádor, J.; Meloni, G.; Selby, T. M.; Osborn, D. L.; Taatjes, C. A. *J. Phys. Chem. A* **2009**, *113*, 1278−1286.
(41) Altarawneh, M. A.; Al-Muhtaseb, H.; Almatarneh, M. H.; Poirier, R. A.; Assaf, N. W.; Altarwneh, K. K. *J. Phys. Chem. A* **2011**, *115*, 14092−14099.
(42) Yasunaga, K.; Kubo, S.; Hoshikawa, H.; Kamesawa, T.; Hidaka, Y. *Int. J. Chem. Kinet.* **2008**, *40*, 73−102.
(43) Rosado-Reyes, C. M.; Tsang, W. *J. Phys. Chem. A* **2012**, *116*, 9825−9831.
(44) Oehlschlaeger, M. A.; Davidson, D. F.; Hanson, R. K. *Proc. Combust. Inst.* **2005**, *30*, 1119−1127.